ISSN: 2834-7706

Research Article

Journal of Mathematical Techniques and Computational Mathematics

Correspondence of Concept of Circular Orbits in Schwarzschild Metric and Kerr Metric to those in Tidally Evolving Binaries in Weak Gravitational Regime and its Application in Determination of Spin of Supermassive Black Hole

Bijay Kumar Sharma*

Electronics and Communication Engineering Department, National Institute of Technology, India

***Corresponding Author**
Bijay Kumar Sharma, Electronics and Communication Engineering Department, National Institute of Technology, India.

Submitted: 2024, May 27; **Accepted:** 2024, Jun 18; **Published:** 2024, June 28

Citation: Sharma, B. K. (2024). Correspondence of Concept of Circular Orbits in Schwarzschild Metric and Kerr Metric to those in Tidally Evolving Binaries in Weak Gravitational Regime and its Application in Determination of Spin of Supermassive Black Hole. *J Math Techniques Comput Math, 3*(7), 01-22.

Abstract

This paper rederives diameters of the Innermost Stable Circular Orbits (ISCO) in Schwarzschild Metric (RDISCO = 6RSch for non-rotating BH with a =0) and in Kerr metric with particular reference to recently studied Super Massive Black Hole in NGC1365 (RDISCO = 9RSch for retrograde orbits and RDISCO = 1RSch for prograde orbits around maximally spinning BH of a=1). Next the same derivations are made in tidally evolving binaries based on kinematic model. Kinematic Model derivation corresponds to the derivations made in Kerr Metric for Circular Orbits in all its details at weak gravitation regime. At strong gravitation regime in Kerr metric, the two orbits converge to Innermost Stable Circular Orbit due to the Space-Time Curvature and Frame-Dragging Effect in the vicinity of SMBH. Kinematic model fails to arrive at ISCO since it has not included the relativistic mechanics.

1. Introduction

1.1 Innermost (Marginally) Stable Circular Orbit Around a Spinning Super-Massive Black Hole (SMBH)

Practically all massive Galaxies are anchored by Super Massive Black Holes (SMBH). These SMBH are placed at the astrometric center of the Galaxy but these centers, including our Milky Way center, is highly shrouded by gas and dust and hence completely obscured from Optical Telescope view. But mm/sub-mm astronomy, particularly at 1.3 mm, gives a clear view of these shrouded SMBH behemoths of energy which power all the distant QUASERS and regulate the growth of all massive Galaxies. Hence Radio Astronomy became indispensible for unraveling the genesis and evolution of our Universe.

In Cambridge, Massachussetts, Harvard-Smithsonian Center for Astrophysics (CfA) has been established for the study of the origin, evolution and ultimate fate of the Universe. It is a joint collaboration between Smithsonian Astrophysical Observatory and the Harvard College of Observatory. CfA Scientists are organized into six research divisons to unravel every aspect of our evolving Universe.

The team has used a technique called Very Long Baseline Interferometry, or VLBI, which links data from radio dishes located thousands of miles apart. Signals from the various dishes, taken together, create a "virtual telescope" with the resolving power of a single telescope with aperture size as big as the space between the disparate dishes . The technique enables scientists to view extremely precise details in faraway galaxies. VLBI array consists of four telescopes at four geographical locations. First is James Clerk Maxwell Telescope (JCMT) on Mount Kea at Hawaii. Second is Arizona Radio Observatory Submillimeter Telescope. Third location has two telescopes of the Combined Array for Research in Millimeter Wave Astronomy (CARMA) 60 m apart in California. This has a combined resolution of 6RSch (6 times the Schwarzschild Radius of Sagittarius A* the SMBH at the center of our Galaxy-Milky Way).Through an International Collaboration of Europe, USA and E. Asia an advanced and upgraded VLBI is coming up in N.Chile on Atacama Plataeu known as Atacama Large mm/sub-mm Array (ALMA). This will be integrated with the existing VLBI to assemble an Earth-size Virtual Telescope known as Event Horizon Telescope. This international Collaboration is led by ESO (on behalf of Europe), National Radio Astronomical Observatory (on behalf of N.America) and National Astronomical Observatory of Japan (on behalf of E.Asia).

The above International Collaboration, ALMA, has upgraded

the VLBI instrumentations in June 2014 by installing an Ultraprecise Atomic Clock in the heart of the Supercomputing Correlator at ALMA's Array Operator Site. This Ultraprecise Atomic Clock is powered by Hydrogen MASER. Hydrogen MASER (Microwave Amplification by Stimulated Emission Radiation) produces a pure monochromatic beam of microwave from which perfectly periodic Clock Pulses are derived. The Global Array of mm and sub-mm Radio Telescopes are synchronized through these periodic Clock Pulses. This accurate synchronization will convert the Global Array into Earth-size Virtual Telescope and has been named Event Horizon Telescope (EHT). This will have Earth-size aperture and ultra-precise time keeping. Presently observations are carried out at 1.3mm but efforts are aimed at observing at 0.87mm. EHT will achieve a resolution better than 20μarcsecond. These ALMA systems have digital baseband technologies. High Band-Width Digital Signal Processors are used to filter VLBI data streams. The signals from the phased array Antennas are time stamped and encoded by a dedicated Atomic Clock. These are recorded on custom built banks of Hards Disk Drives. The data from ALMA and similar data from other Radio Network Nodes are shipped to the Central Processing Center where identically timed signals are combined for analysis. A continuous data throughput of 16Gb/s been achieved using Field Programmable Gate Array (FPGA) computational platform and the goal is to achieve 64Gb/s. The difference between the existing VLBI and EHT is the geographical spread, extension to shorter wavelength of operation and addition of unprecedented collecting area enabled by phased ALMA.

The SMBH at the center of M87 which has Schwarzschild Radius (RSch) of 5.93479×10-4pc and which is located at D =16.7±0.6 Mpc from Earth subtends 2×7.33013 μarcsecond on Earth. SMBH at the center of our Galaxy, namely SgrA*, also subtends an angle of a similar range. Hence EHT will be up to the task of studying the details of the Space-Time around the boundaries of BH which is known as Event Horizon. BH strong gravity leads to gravitational lensing which in turn leads to the annular brightening of the last photon orbit (the innermost stable orbit of photon around BH). The last Photon Orbit creates a BH shadow as shown in Figure 1: The size and shape of the BH shadow is predicted by Einstein's GR and it depends on the mass and spin of BH. The final goal of EHT is to spatially resolve Space-Time fabric in the Event Horizon Region of the BH which will enable the verification of GR in truly strong gravitation regime, develop models of BH growth and develop models of triggering Relativistic Jets and Radiation along the polar axis of BH.

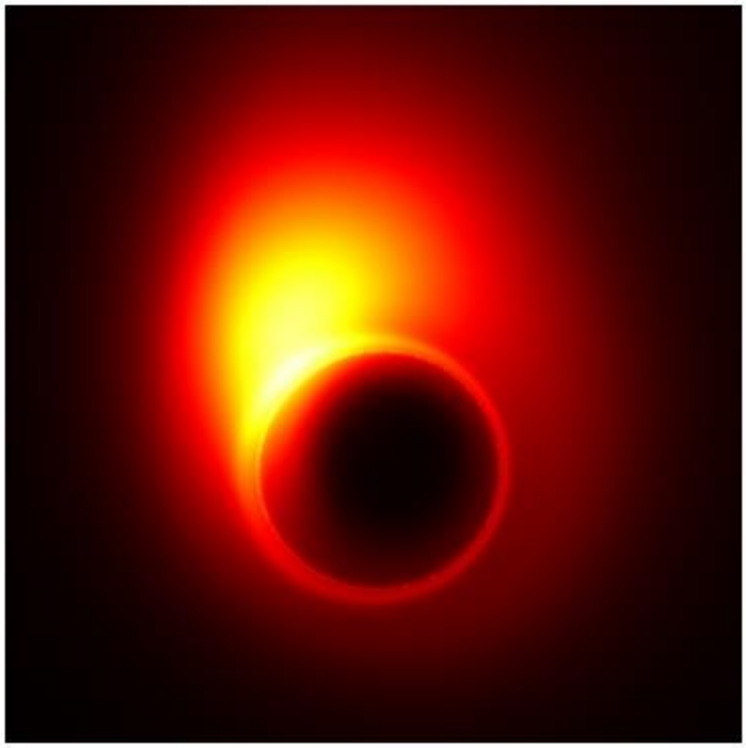

Figure 1: This Image, Created Using Computer Models, Shows How the Extreme Gravity of the Black Hole in m87 Distorts the Appearance of the Jet Near the Event Horizon. Part of the Radiation From the Jet is bent by Gravity Into a Ring that is Known as the 'Shadow' of the Black Hole. Credit: Avery e. Broderick (Perimeter Institute & University of Waterloo)

Using VLBI, Doeleman et.al. and his team studied the SMBH in the Galaxy M87 and measured the diameter of inner edge of the accretion disk to be only 5.5 times the size of the black hole event horizon i.e. 5.5RSch [1]. A retrograde accretion disk will have an inner diameter greater than 7.35RSch on account of Lense-Thirring effect or Frame Dragging Effect . According to the laws of physics, the observed size of 5.5RSch suggests that the accretion disk is prograde and spinning in the same direction as the black hole-the first direct observation to confirm theories of how black holes power jets from the centers of galaxies.

1.2 Accretion Disk

Every Galaxy has SMBH at the center. This SMBH regulates the growth as well as it anchors the massive Galaxy. SMBH can be in active stage or in quiescent stage. Because light cannot escape from SMBH and because the light from outside just wraps around SMBH hence we see a dark shadow. So the best way to study SMBH is to study the activities going on outside the boundary of SMBH. If it is active, the swirling mass of gas and dust will become the basis of studies and if SMBH is in quiescent stage, as Sgr A* is, then the tidally disrupted star within its tidal disruption Radius will become the basis of investigation [2].

When SMBH is in active stage the galaxy is referred to as Active Galactic Nuclei (AGN). The viewing angle decides the luminosity of the Galaxy and accordingly it is classified.

10% of AGN exhibit collimated relativistic jets which are produced by the accretion of stars, gas and dust [1]. These powerful collimated jets of relativistic particles can extend for hundreds and thousands of light years and terminate into radio lobes with minimum energy stored being 1060-64 Ergs. These provide an important mechanism for redistributing matter and energy on large scales that affect evolution of Galaxies. If we happen to be looking down the collimated relativistic jet then we classify AGN as Blazer. At 30º angle or less with respect to the collimated relativistic jet we see a luminosity in excess of 1011LΘ . Such an AGN is classified as QUASER/Seyfert 1. Here LΘ is the luminosity of sun-size star. If our line-of-sight is at 60º angle or more or if we have an edge-on view with respect to the AGN, then it is classified as Seyfert 2/Radio Galaxy. AGN viewed from different angles is illustrated in Figure 2 [3].

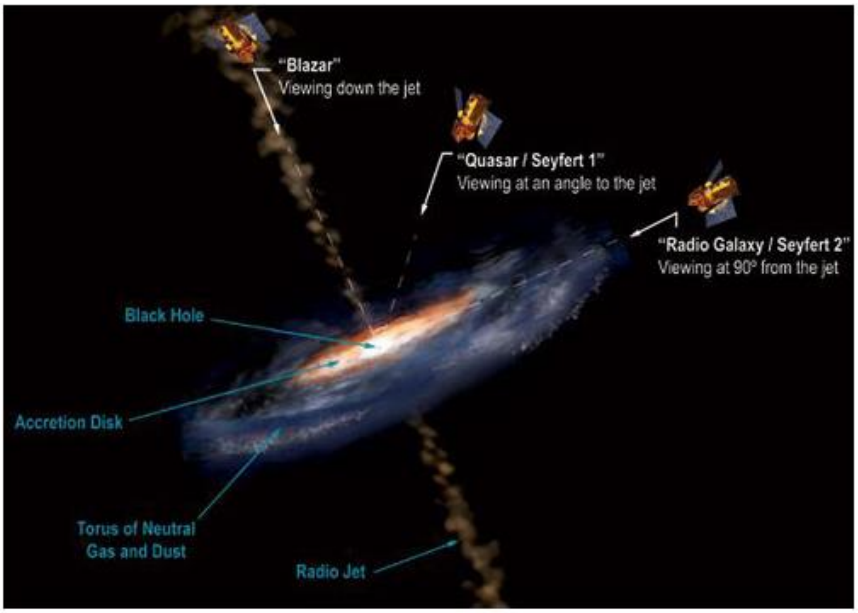

Figure 2: AGN at Various Angles – Blazer (Looking Down the Jet), QUASER/Seyfert 1(Viewing at Angle of 30º or Less) and Radio Galaxy/Seyfert2 (at an Edge-On View of AGN).Credit: Aurore Simonnet, SSU NASA E/PO

Cool gas in the filaments of the Cosmic Web of our Universe is continuously being channeled into the intersections of the filaments [4]. At these intersections, large Dark Matter (DM) halo reside and in these DM halo the galaxies are built up. As the gas cools and becomes dense, it fragments and collapses into first stars. Simultaneously a cluster of stars merge to form the Intermediate Mass Black Holes (IMBH). These have a mass of 102~105MΘ [5].

IMBH grow by accreting the surrounding gas. This could be a gradual process in which the in-falling material is compressed into an accretion disk and heated to high temperature. In the process it outshines all the stars in the host galaxy. The full grown accreting IMBH after attaining a mass of 106MΘ to 109MΘ are called SMBH and accreting SMBH are called QUASERS - a radiative manifestation of SMBH. The central compact region of the QUASER is behemoth of energy and is powered by accreting SMBH. The conversion of gravitational energy into Radiation, collimated Relativistic Jets of particles shooting along the polar axis of SMBH and gas wind on disc side through accretion on the SMBH is the plausible explanation of high output power from such compact volume of the Active Galactic Nuclei. Mass accretion by IMBH is limited by Eddington Limit Luminosity. Rate of accretion is opposed by Radiation Pressure. If Luminosity exceeds a critical value described by Mass then the star will blow up. Eddington limited accretion is too slow to allow stellar-mass BH seeds of 10 MΘ to grow into Super Massive Luminous Quasers that are observed 1by after the Big Bang. The way out of this impasse is that Pop III remnant BH seed is embedded in a nuclear star cluster fed by dense cold gas flows from the filaments of the cosmic web [6]. Low mass stellar BHs are trapped in ubiquitous dense cold gas flows at $z > 1.5$. These are launched by stellar dynamical processes into a phase of supply-limited, supra-exponential accretion. These rapidly grow in a few tens of Mega years into greater than 104MΘ BH seeds. Subsequent slower Eddington limited growth by disk accretion suffices to produce SMBH that power the brightest early QUASERS.

Over a billion of years by accreting stars and gas, by major and

minor mergers, by chaotic and coherent mergers, IMBH evolve into SMBH (>105MΘ) and also drift to the central position of the Galaxy providing kinematic stability to the galaxy as a whole. The central position is the bottom of the potential well of the Galaxy and the dynamical friction drag causes the SMBH to drift to the central position. This is exactly in line with Primary-centric Architecture proposed by the Author [7].

Evolution of IMBH into SMBH and the subsequent evolution of SMBH causes the accretion of interstellar material over cosmic time. Accretion process liberates huge amount of energy in form of radiation as observed in QUASERS or as energetic gaseous outflow and collimated relativistic particle jets moving along the polar axis of the SMBH as seen in 10% of AGN. Through the production of Winds and Jets, SMBH seeds the surrounding with matter and energy. Such heating of the ambient gas in and around the Galaxy plays a significant role in regulating the Star Formation Rate.

This enormous energy input from evolving SMBH can either blow gas out of the galaxy completely and thus quench the subsequent star formation rate (SFR) or can reheat the surrounding gas. This stops any further flow of cool gas into the intersection of filaments and stops the ongoing SFR [8].

Thus SMBH acts as a thermostat regulator which initially leads to the redistribution of matter throughout the galaxy which leads to continued SFR in the bulge. But eventually it shuts off the runaway SFR and maintains Central Bulge Mass to SMBH Mass ratio at 1000:1. This type of feedback has been linked to the potential explanation for the famed M-σ relation where M is the mass of SMBH and σ is the spread in the velocities of stars in the central bulge [5,9].

There is angular momentum transfer from the accreting matter to the spinning SMBH. When the spin of SMBH gets sufficiently large, greater than 0.93, then the spin regulates the galaxy growth on scales far beyond its gravitational sphere of influence. This is because at this point the collimated Jets are launched by the magnetic extraction of rotational energy from the ergo-sphere of the BH [10].

1.3 The Inner Edge of the Accretion Disk is ISCO (Innermost Stable Circular Orbit) and its Relation to the Spin of SMBH

In AGN, SMBH is in ON condition. The surrounding gas and dust are continuously swirling around the BH. These surrounding matter does not fall into the BH instead it tightly orbits the BH. Orbiting gas and dust and proximal stars very near ISCO get blocked at ISCO and matter builds up into a flat pancake. As seen in Figure 3, there is a shallow potential energy valley at ISCO and hence ISCO is referred to as marginally stable. In this shallow potential valley the swirling mass piles up to form the inner edge of the flat pancake. This flat pancake is defined as Accretion Disk. The inner edge of the Accretion Disk is defined as Innermost Stable Circular Orbit (ISCO) as shown in Figure 3.

Figure 3: This Artist's Impression of the Innermost Regions of M87 Shows the Relationship between the Black Hole, the Orbiting Accretion Flow, and the Launching of the Relativistic Jet. Credit: Perimeter Institute for Theoretical Physics

The matter at the inner edge may be perturbed into orbits shorter than ISCO. This gets launched on a collapsing spiral or death spiral because it ends up as the feedstock of the gluttonous SMBH. Gravitational interaction with the neighbouring Galaxies can trigger the in-spiral or the death spiral from the inner rim of the accretion disk. But normal, undisturbed Galaxies also host powerful QUASERS which is the radiative manifestation of mass accretion by central SMBH. In these undisturbed Galaxies what triggers the mass accretion is still under investigation.

So the overall picture is that the accretion disk is orbiting around the spinning SMBH at nearly the speed of light and is providing a steady diet of superheated material to the SMBH. The mechanism of accretion onto the SMBH is a complex Magneto Hydro Duynamic (MHD) process which is yet to be fully understood. The Gravitational Waves radiated during the matter accretion could have given a robust measure of the spin parameter of SMBH. But the detection of Gravitational Waves of this order will have to wait for another decade. In the absence of detecting the Gravitational Wave Signatures we are left with the only option of measuring the Electro-Magnetic Waves emitted from the accretion disk or reflected from the inner edge of the Accretion Disk. GR predicts several Relativistic Signatures in the Radiation close to the Event Horizon. Frame Dragging (Lense-Thirring Effect) and Gravitational Time Dilation leading to Gravitational Redshift should leave its imprint on radiation from these regions.

Accretion Disk radiates as a Black Body with Spectral Density peak at $\lambda Wien = 0.1\mu m$ (EUV). But inverse comptonization effect by the surrounding plasma uptranslates EUV into X-Ray Band. In smaller Galactic IMBH, the accretion disk is hotter and its $\lambda Wien$ = few Angstroms corresponding to X-Ray band. This X-Ray emission adds to the X-Ray produced by Inverse Comptonization. Thus, X-Ray provide the cleanest probe of the spin of SMBH and these can be studied only through Space X-Ray Telescope such as NuSTAR and XMM-Newton.

EXOSAT was launched in 1983 by ESO and it surveyed in the energy range of 1 to 50keV. It made detailed observation of Quasi-Periodic Oscillations in several low mass X-Ray Binary Systems [11]. It carried spectral survey of 48 Seyfert Galaxies. These spectrum contained soft X-Ray component of Seyfert Galaxies [12]. These soft component was thought to represent disk emission in accordance with the theory that postulated AGN as SMBH/disk related events.

Both EXOSAT (launched by ESA) and Ginga (launched by Japanese Space Organization) discovered Iron-line emission and Inverse-Comptonization hump in SMBH X-Ray Spectra [13].

ASCA (Advanced Satellites for Cosmology and Astrophysics) was an updated X-Ray Telescope jointly launched by USA and Japan in 1993. It had a imaging capability with a broad pass-band filter, moderately high X-Ray resolution ($E/\Delta E \sim 100$) and a larger effective area. It was first to employ Charge-Coupled Device and an X-Ray Detector. ASCA made the study of Iron-Emission line precise. ASCA established that it was a highly prevalent feature in Seyfert-1 sources and it could be used to constrain SMBH Spin.

In 1995, Rossi X-Ray Timing Explorer (RXTE) was launched to study the X-Ray Spectral and Temporal variability in BH Systems and in the process it made detailed study of the accretion disks. In 1999, ESA launched XMM-Newton Observatory and NASA launched Chandra-X-Ray Observatory. Chandra excels in precision X-Ray imaging whereas XMM-Newton Observatory has a larger collection area and suitable for X-Ray Spectroscopy. This has enabled the study of accretion and radiation in high-gravity regime next to the event-horizon of a given SMBH. These two Telescopes have enabled to unravel the complex interactions between SMBH and its accretion disk [14,15]. Detailed characterization of the emission features from the disk are providing reliable constraints on SMBH Spin [16].

In 2004, SWIFT had been launched. This is suited for examining the X-Ray spectrum in the range of 0.2 – 10 keV. This covers the continuum and Kα Iron-line invariably found in AGN and SMBH. In 2005, SUZUKA has been launched. This records the X-Ray spectrum over a wide range from 0.3 to 600keV with enhanced resolution [17,18]. This has enabled Scientists to identify the distortion in the Iron-line and the hard X-Ray hump due to the spin of the centrally placed SMBH as shown in Figure 4.

Gamma Ray Large Area Space Telescope (GLAST) renamed as Fermi Gamma Ray Space Telescope (FGST) was launched on 11th June 2008 as a joint venture of NASA, USA Department of Energy, Space Agencies of France, Germany, Italy, Japan and Sweden. It has carried out deeper study of High Energy COSMOS from Super Massive Black Holes in distant galaxies to thunderstorms on Earth. It discovered Giant Bubbles towering above and below to a height of 25,000lys. It is looking into high energy processes from Pulsars within our Galaxy to Relativistic Collimated Jets powered by SMBH in far away young galaxies. An unique view is obtained of the transfer of angular momentum from the swirling in-spiraling gas, dust and star to the central SMBH, of the disk jet interactions and of the jet triggering mechanisms.

NuSTAR (Nuclear Spectroscopic Telescope Array) was launched on June 13,2012, as aSmall Explorer mission led by Caltech and managed by NASA's Jet Propulsion Laboratory in Pasadena, California, for NASA's Science Mission Directorate in Washington. It has completed its Primary Mission and is now on a two-year extended mission. It looks at high energy X-Ray beyond the present space X-Ray telescope capabilities. The survey of High Energy Universe in X-Ray and Gamma-Ray band is revealing how heavier elements were formed and seeded throughout the Universe as we know today. SWIFT, Chandra X-Ray Telescope and Nu-Star complement one another and together they provide a complete data set in the X-Ray band of the spectrum. Fermi added data in higher energy γ-band. NuSTAR mission is dedicated to the observations of target of opportunity which have been detected as targets of high opportunity by other space observatories and by ground based

observatories. NuSTAR confirmed that SMBH, NGC 253, in Sculptor Galaxy has gone dormant but the Galaxy is the nearest Star Burst Galaxy. This is rather unusual and it will be resolved in future by constant monitoring. The physics of SMBH tells us the where Star Formation Rate is high there SMBH is gluttonously devouring the surrounding gas, dust and stars leading to enormous temperature and enormous X-Ray emission.

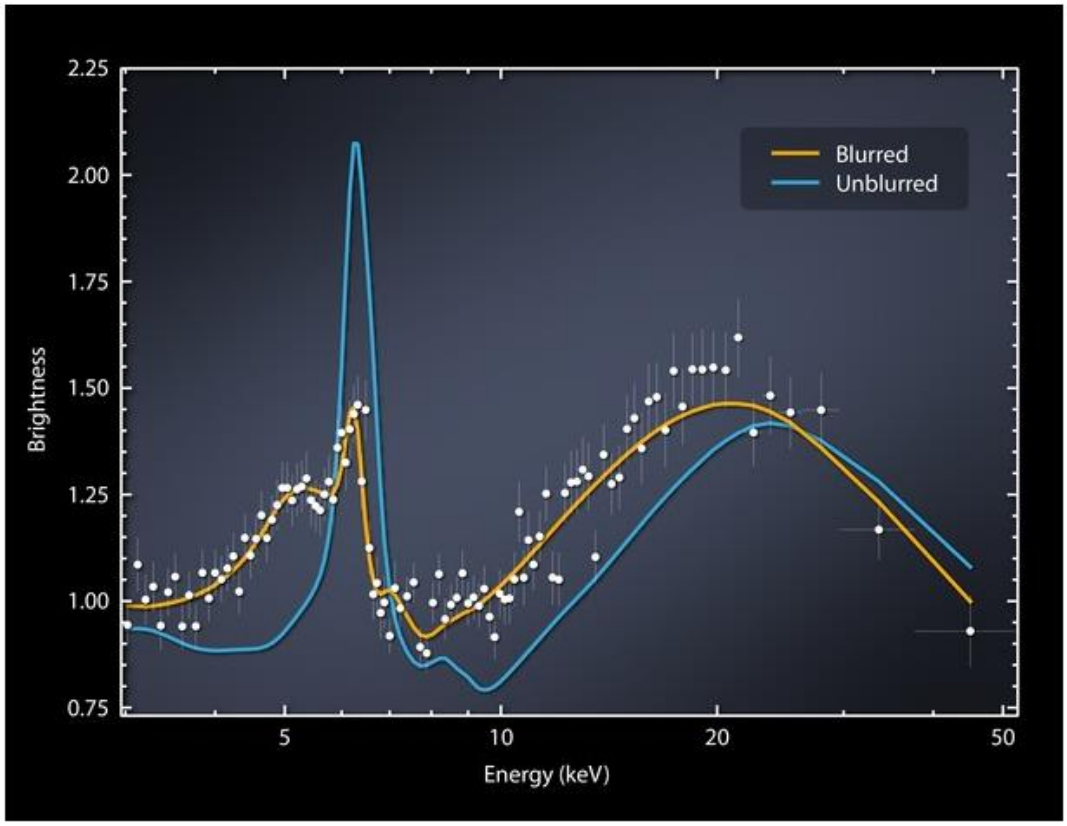

Figure 4: X-ray Light Streaming from Regions Near a Supermassive Black Hole Known as Markarian 335

The yellow line is a model that shows what the data are predicted to look like if X-ray light has been distorted by relativistic reflections. The blue line shows what the plot would look like without distortions. The white dots show the actual NuSTAR data, indicating the light is extremely distorted due to Relativistic Reflections. Credit NASA/JPL-Caltech/Institute for Astronomy, Cambridge.

The plot of data in Figure 4 has been captured by NASA's Nuclear Spectroscopic Telescope Array, or NuSTAR. It shows X-ray light streaming from regions near a supermassive black hole known as Markarian 335 [19]. The light is coming from two areas: a superheated disk of material feeding the black hole, called the accretion disk shown in Figure 3; and a cloud of particles traveling near the speed of light, called the corona. The exact shape and nature of coronas are not clear, but researchers know that X-ray light from the corona is reflected off the accretion disk. The reflected light, and the corona's direct light, are mapped in this plot over a range of X-ray energies. (This is the highest range of X-rays, which NuSTAR was specially designed to see).

Why does this distortion of the X-Ray light occur ? First, there is a Doppler shift happening due to the spinning accretion disk. As one side of the accretion disk moves toward us and the other side away, the light is squeezed or stretched. A second effect has to do with the enormous speeds of the spinning black hole, which approach the speed of light and which causes Frame-Dragging Effect or Lense-Thirring Effect. A final effect is from the enormous gravity of the black hole, and the subsequent Space-Time bending which pulls on the light, making it harder to escape its grasp. The light loses energy in this process. All of these factors contribute to the distortion as seen in the plot.

The data in Figure 4 were taken after a dramatic dip in brightness had first been observed by NASA's Swift satellite [19]. NuSTAR's high-energy X-ray data pointed to the cause for the observed change: Markarian 335's corona had shifted closer to the black hole itself -- and this closer proximity meant that the black hole's gravity could yank harder on the corona's light, stretching it to lower energies than observed before. The astronomers say that the corona moved over a period of days, and is still in the close configuration. They don't know if and when it would move back to where it was previously, or why the corona moved. NuSTAR and other high-energy telescopes are busy trying to crack these mysteries.

In December 2009, NASA launched Wide Field Infra Red Survey Exploration (WISE). It has led to the discovery of Dust Obscured Galaxies (DOG). Daniel Stern et.al. have discovered

million such dusty BH candidates and 1000 even dustier objects thought to be among the brightest galaxies and are referred to as hot DOGs [20]. In another study which is yet to appear WISE has identified 2.5 million actively feeding SMBH across the full sky stretching back to 10bly. The IR bump betray the BHs.

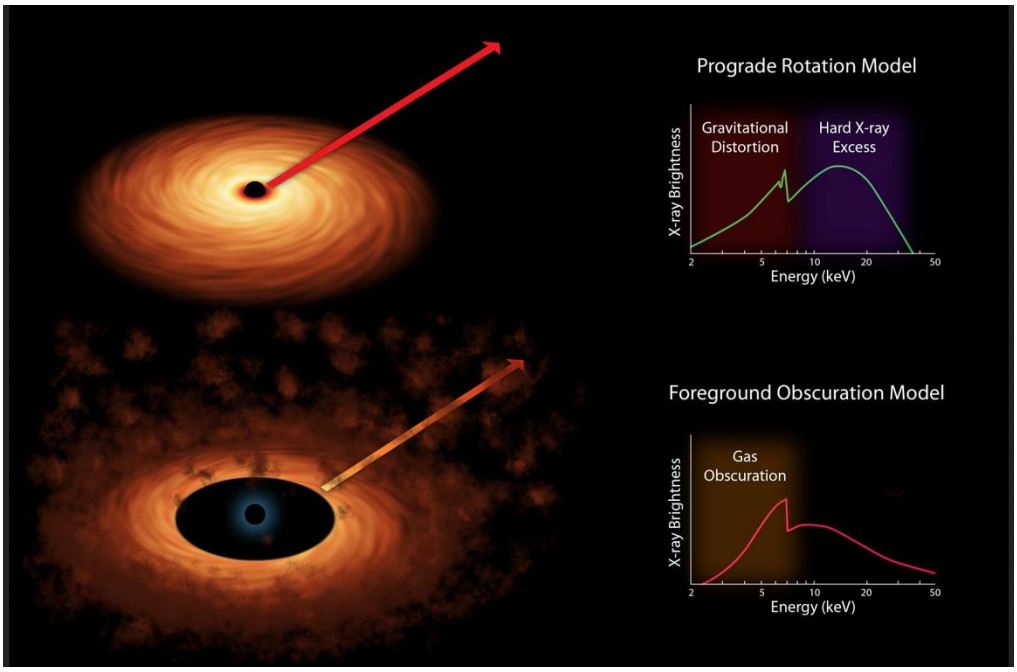

Figure 5: Scientists measure the spin rates of supermassive black holes by spreading the X-ray light into different colors. The light comes from accretion disks that swirl around black holes, as shown in both of the artist's concepts. They use X-ray space telescopes to study these colors, and, in particular, look for a "fingerprint" of iron-the peak shown in both graphs, or spectra- to see how sharp it is. Prior to observations with NASA's Spectroscopic Telescope Array, or NuSTAR, and the European Space Agency's XMM-Newton telescope, there were two competing models to explain why this peak might not appear to be sharp. The "rotation" model shown at top held that the iron feature was being spread out by distorting effects caused by the immense gravity of the black hole. If this model were correct, then the amount of distortion seen in the iron feature should reveal the spin rate of the black hole. The alternate model held that obscuring clouds lying near the black hole were making the iron line appear artificially distorted. If this model were correct, the data could not be used to measure black hole spin. NuSTAR helped to solve the case, ruling out the alternate "obscuring cloud" model. Its high-energy X-ray data-shown at top as green bump to the right of the peak-revealed that features in the X-ray spectrum are in fact coming from the accretion disk and not from the obscuring clouds. Together with XMM-Newton, the space observatories were able to make the first conclusive measurement of a black hole's spin rate, and more generally, confirm that the "gravitational distortion" model is accurate. Image credit: NASA/JPL-Caltech

Nuclear Spectroscopic Telescope Array (NuSTAR).
Through X-Ray Telescopes (ESA's XMM-Newton Observatory and NASA's Nuclear Spectroscopic Telescope Array (NuSTAR)), Risaliti et.al. measured the high energy light emitted by iron atoms from the center of the Galaxy [21]. This enabled them to measure the radius of rim of accretion disk. From this rim radius the spin parameter of NGC1365 was extracted.

2. Effective Potential in Schwarzschild Metric

The Schwarschild metric is the most general spherically symmetric vacuum solution of the Einstein field equations.

$$V(r) = \frac{\epsilon \times c^2}{2} - \frac{\epsilon \times c^2 (\frac{GM}{c^2})}{r} + \frac{L^2}{2r^2} - \frac{GML^2}{r^3} \quad 1$$

= constant term + Newtonian Potential Term + Contribution of Angular Momentum+ General Ralativity term;
In (1),

$$Constant\ term = \frac{\epsilon}{2}; Newtonian\ Potential = -\frac{\epsilon GM}{r};$$

$$Contribution\ of\ Angular\ Momentum = \frac{L^2}{2r^2}; GR\ contribution = \frac{GML^2}{r^3};$$

Let 2GM = gravitational radius/Schwarzschild radius = rG assuming 'c'=1.
For massive particles, ε = 1 and 2GM is replaced by gravitational radius/Schwarzschild radius = rG and let radial parameter be normalized as x = r/ rG.
Hence (1) becomes:

$$V(x) = \frac{1}{2} - \frac{1}{2x} + \frac{(\frac{L}{r_G})^2}{2x^2} - \frac{(\frac{L}{r_G})^2}{2x^3} \quad (2)$$

Differentiate (2) with respect to 'x' and we get:

$$\frac{\delta V}{\delta x} = \frac{3k}{2x^4} - \frac{k}{x^3} + \frac{1}{2x^2} \qquad where\ k = (\frac{L}{r_G})^2 \quad (3)$$

Equating the first derivative of V(x) to zero we get the roots where extremums of V(x) occur.
These roots are:

$$x_{max} = k + \sqrt{-3k + k^2} \ \ and\ x_{min} = \ k - \sqrt{-3k + k^2} \quad (4)$$

These roots are real and coincident at k = 3.
For k = 3, the roots are coincident at x = 3.

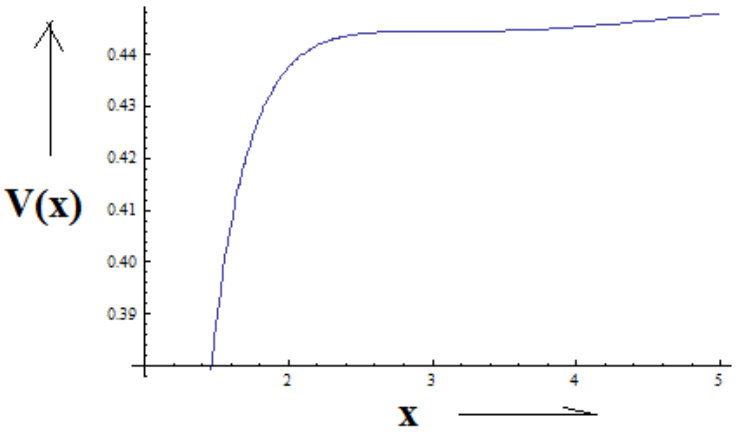

Figure 6: Potential Profile of a Massive Particle with a Marginally Stable Orbit at x = 3.

For k= 4 the roots are at x=2 and x=6.
V(x) has a MAXIMA at x=2 and MINIMA at x=6 as shown in Figure 2.

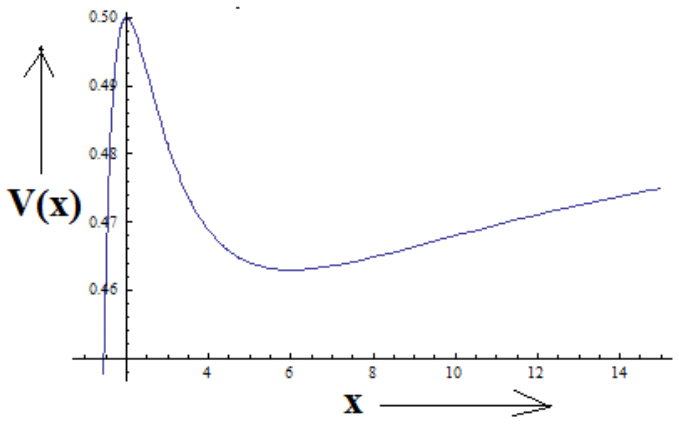

Figure 7: Maxima at x= 2 Corresponding to Unstable Orbit and Minima at x = 6 Corresponding to Stable Orbit

For k = 1,000,000 the roots are x = 1.5 and x = $^{2\times106}$. Here again the inner root x = 1.5 is the MAXIMA of V(x) and the outer root x = 2×10^6 is the MINIMA of V(x).

This analysis clearly shows that at x = 3, i.e. at r = 3× r_G, we have the innermost marginally stable circular orbit known as ISCO (innermost stable circular orbit). As L increases beyond (√3) r_G, the roots are split up in inner unstable circular orbit and outer stable circular orbit.

With increase in L, the inner unstable orbit converges to r = 1.5× rG and outermost stable orbit goes on increasing indefinitely. Hence it will be valid to say that Innermost Stable Circular Orbit(ISCO) which is really MARGINALLY STABLE only as is evident from Figure 1 lies at r = 3× r_G. In strict sense of the word, r = 3× r_G is a meta-stable orbit which is being referred to as marginally stable.

3. ISCO for Photons in Schwarzschild Metric

For Photons, constant term and Newtonian Potential term in (2) does not exist. Gravitational lensing is done by the fourth term. Hence (2) is rewritten as:

$$V(x) = \frac{(\frac{L}{r_G})^2}{2x^2} - \frac{(\frac{L}{r_G})^2}{2x^3} = \frac{k}{2x^2} - \frac{k}{2x^3} \qquad where\ k = (\frac{L}{r_G})^2 \tag{5}$$

Differential of (5) with respect to 'x' is:

$$\frac{\delta V}{\delta x} = \frac{3k}{2x^4} - \frac{k}{2x^3} \tag{6}$$

Equating (6) to zero we get a root at x = 1.5. This corresponds to a potential peak as shown in Figure 3.

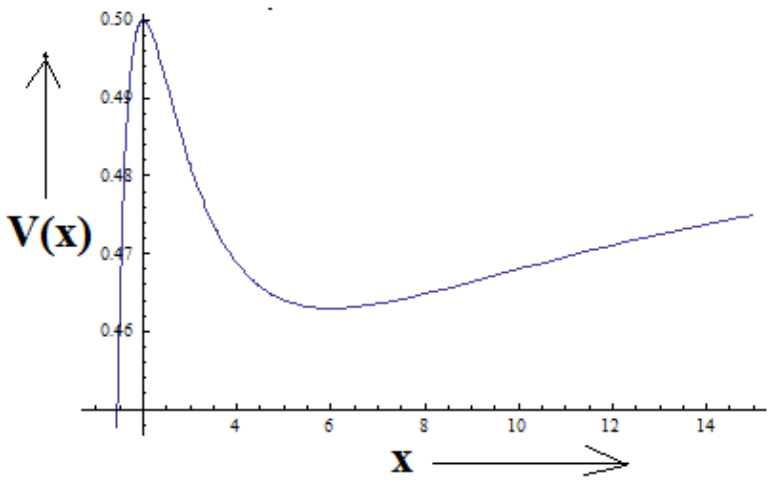

Figure 8: Potential Energy Profile for a Photon. For any Angular Term i.e.for any k there is a peak at x = 1.5. For this profile k =4

For any L, there exists a Potential energy peak at x = 1.5. This peak acts as barrier to photons. This peak also implies that at x = 1.5 or r =3×GM there is an unstable circular orbit of Photon. Photon gets wrapped around the black Hole at r = 3×GM. Hence there is a shadow in the sky in the position of the Black Hole.

4. Stable Circular Orbits around Rotating Black Holes

We have used the Euler-Langrange formalism to find the geodesics (orbit equations) for the Schwarzschild metric. We can find the geodesics for the Kerr metric in a similar way. We can then go through the effective potential treatment and find the types of orbits.

Kerr metric or Kerr geometry describes the geometry of empty spacetime around a rotating uncharged axially symmetric black hole with a quasi spherical event horizon. The Kerr metric is an exact solution of of the Einstein Field equations of General Relativity.

The space-time outside a Black Hole with gravitational mass M, Charge Q and angular momentum a = J/M is described by the Kerr Metric given in Eq.(7).

The generalized form of effective potential is:

$$\text{Veff}\,(r,\alpha) = -\kappa\frac{M}{r} + \frac{l^2 - a^2(\varepsilon^2-1)+Q^2}{2r^2} - \frac{M}{r^3}(l-a\varepsilon)^2 + \frac{Q^2}{r^4}(l-a\varepsilon)^2$$

Here α =(M, Q, a, ε, t)
= a collection of parameters of Black Hole and test particle.
All the parameters in the equation describing Veff (r,α) are described in the paper
arXiv:1706.05466 v2(gr-qc)

In the limit Q=0
The effective potential for Kerr Metric is the following:

$$V_{eff} = -\kappa\frac{M}{r} + \frac{l^2 - a^2(\varepsilon^2-1)}{2r^2} - \frac{M}{r^3}(l-a\varepsilon)^2 \qquad 7$$

= rotating body exhibits frame-dragging (also known as Lense-Thirreing
precession) a distinctive prediction of General Relativity;

Here l is the conserved angular momentum per unit mass of the test particle, and ε is the conserved energy per unit mass of the test particle, and where κ = 0 for light ray geodesics and κ = 1 for massive particles.

L*/m = l = the conserved angular momentum per unit mass of the test particle and
E*/m = ε = the conserved energy per unit mass of the test particle.
The spin parameter 'a' =(cJ*/(GM^2)) is given as a Dimensionless parameter.
We are going to convert M(kg), l(m^2/s), a (dimensionless) in parameters of LENGTH dimension and ε(Joules/Kg) in a dimensionless parameter by the conversion rules given in Table 1. This achieves the Dimensional Balance in (7).

Parameter	Conversion Rule
M(Kg)	M(kg)×0.7425×10^{-27}(m/Kg)
l (m^2/s)	l (m^2/s)/c(m/s)
a = (cJ*/(GM^2))Dimensionless	a×GM(m^3/s^2)/c^2(m/s)^2
ε(Joules/Kg)→(m^2/s^2)	ε(m^2/s^2)/ c^2(m/s)^2

Table 1: Conversion Rules

4.1 Consider the Rapidly Spinning Black Hole in NGC 1365 [22-24]

Done et.al. have extensively studied the SMBH (Super Massive Black Hole) at the center of the NGC1365 [24]. A black hole's gravity is so strong that, as the black hole spins, it drags the surrounding space along. The edge of this spinning hole is called the event horizon. Any material crossing the event horizon is pulled into the black hole. Inspiraling matter collects into an accretion disk, where friction heats it and causes it to emit X-rays.

The team measured X-rays from the center of NGC 1365 to determine where the inner edge of the accretion disk was located. This Innermost Stable Circular Orbit – the disk's point of no return – depends on the black hole's spin. Since a spinning black hole distorts space, the disk material can get closer to the black hole before being sucked in.

The system parameters of SMBH at the center of NGC1365 is given in Table 2.

Parameter	Magnitude		Reference
M($\times M_\Theta$)	2×10^6		Done et.al.(2013)
a(spin parameter)	0.84	At 90% confidence level	Done et.al.(2013)
r_G(gravitational radius)(m)	5.91007×10^9	$r_G = (2GM/c^2)$	Calculated
J*(Kg-m^2/s)	2.96173×10^{54}	a= (cJ*)/(GM^2)	Calculated
L*(Kg-m^2/s)	2.54769×10^{53}	From (9)	
E*(Joules)	(mc^2+ 4.28197×10^{36})	From (10)	
m($\times M_\Theta$)	1	Sun like star is the test particle	
B=$\sqrt{}$(G(M+m)) ($m^{3/2}$/s)	1.62968×10^{13}	For use in (9) and (10)	

Table 2: System Parameters of SMBH at the Center of NGC1365.

Table 3 contains the system parameters after being scaled to suitable LENGTH dimension.

Parameter	Magnitude	Reference
M($\times M_\Theta$)	2.95515×10^9m	Calculated
a(spin parameter)(DL)*	2.51178×10^9m	Calculated
r_G(gravitational radius)(m)	5.91007×10^9m	Calculated
J*(Kg-m^2/s)/M(Kg)	2.48223×10^9m	Calculated
L*(Kg-m^2/s)/m(kg)=l(m^2/s)	4.27044×10^{14}m	Calculated
E*(Joules)/m(Kg)=ε(m^2/s^2)	[1+2.39414×10^{-11}](DL)*	Calculated
m($\times M_\Theta$)	1477.58m	Calculated

*DL-Dimensionless

Table 3: Scaled System Parameters in Length (Meter) Dimension

NGC1356 is a great barred Spiral Galaxy at a distance of D= 17.2± 0.8 Mpc from our Earth. Angular Parallex of the size of the Galaxy is 50 arcsecond. This corresponds to a diameter of 4169pc. Therefore the mean radius of the galaxy is about r_{max} = 2000pc.

Suppose Sun-like particle is moving from the edge of the Galaxy towards the SMBH at the center of the Galaxy.

The initial angular momentum of the test particle which is going to be conserved is L*.
By Kepler's Third Law:

$$r^3\Omega^2 = G(M+m) = B^2;\ \ or\ \Omega = \frac{B}{r^{3/2}}\ where\ B = \sqrt{G(M+m)} \qquad 8$$

By definition, the initial angular momentum L* of the test particle moving from the edge of the galaxy (rmax = 2000pc) which is going to be conserved is:

$$L^* = I \times \Omega = mr_{max}^2 \times \frac{B}{r_{max}^{3/2}} = mr_{max}^{1/2} \times B = 2.54769 \times 10^{53} Kg - m^2 - s^{-1} \quad 9$$

Accordingly the total Energy E* of the test particle moving from the edge of the galaxy (rmax = 2000pc) which is going to be conserved is:

$$\begin{aligned} E^* &= rest\ mass\ eqivalent\ energy + \frac{1}{2} I^* \Omega^2 = m \times c^2 + \frac{1}{2} I^* \times \frac{B^2}{r_{max}^3} \\ &= m \times c^2 + \frac{1}{2} \times m \times r_{max}^2 \times \frac{B^2}{r_{max}^3} = m \times c^2 + \frac{1}{2} \times \frac{mB}{r_{max}} \\ &= m \times c^2 + 4.28197 \times 10^{36} Joules \end{aligned} \quad 10$$

Energy per unit mass (ε) is given as follows:

$$\varepsilon = (c^2 + 4.28197 \times \frac{10^{36}}{1.9 \times 10^{30}})(\frac{m}{s})^2 = (c^2 + 2.25367 \times 10^6)\left(\frac{m}{s}\right)^2 \quad 11$$

After applying the conversion rule to scale it and normalize it to Dimensionless quantity we get:

$$\frac{\varepsilon}{c^2} = (1 + 2.39414 \times 10^{-11}) \quad 12$$

We substitute the system parameters given in Table 3 in (7) and differentiate it with respect to 'r'. The first derivative is equated to zero to obtain the extremum points.

The two roots are:

Inner root 'r' = 8.86545×10^9m and Outer root 'r' = 6.17114×10^{19}m.

The Potential Profile at the two roots are given in Figure 4 and Figure5.

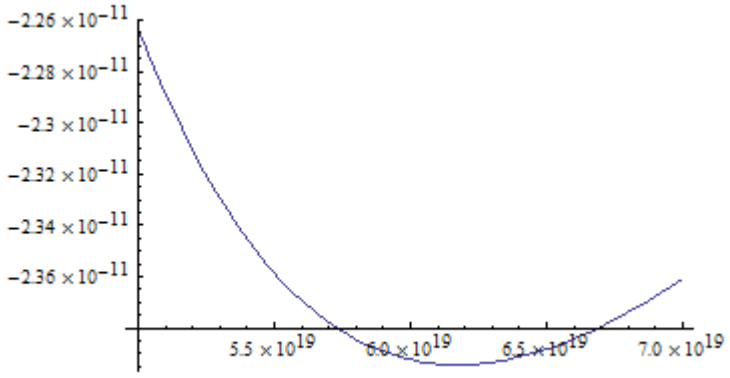

Figure 9: Potential Energy Profile for a Spinning BH with Test Particle Launched from the Edge of the Galaxy Towards the Center of NGC1365. It has a Energy Minima at r = 6.17114×10^{19}m Corresponding to a Stable Circular Orbit

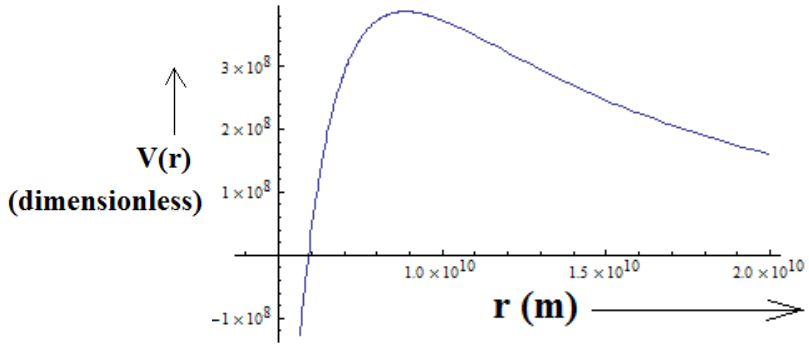

Figure 10: Potential Energy Profile for a Spinning BH with Test Particle Launched from the Edge of the Galaxy Towards the Center of NGC1365. It has a Energy Maxima at r = 8.86545×10^9m Corresponding to a Unstable Circular Orbit

From the analysis of Figure 9 and Figure 10f it is clear that inner Circular Orbit is placed at the maxima of the Potential Energy Profile and hence it is Unstable and Outer Circular Orbit is placed at the minima of the Potential Energy Profile and hence it is the Stable Outer Circular Orbit.

Now we will look for the Innermost Stable Circular Orbit (ISCO). For this we will consider test particles of different L as listed in Table 4.

Distance of Launch From the center	$L^*=mr^{1/2}B$ (Kg-m^2/s)	(l/c)(m)	$E^*=mc^2+(0.5I\Omega^2)$ $= mc^2+(0.5mB/r)$	ε/c^2 (DL)	Inner Unstable CO($\times10^9$m)	Outer Stable CO($\times10^{17}$m)
2000pc	2.54769 $\times10^{53}$	4.27044 $\times10^{14}$	mc^2+4.28197 $\times10^{36}$	1+2.39414 $\times10^{-11}$	8.86545	617.114
10pc	1.8×10^{52}	3×10^{13}	$mc^2+8.56\times10^{38}$	$1+4.8\times10^{-9}$	8.86398	3.08558
5pc	1.27×10^{52}	2.13×10^{13}	$mc^2+1.7\times10^{39}$	$1+9.6\times10^{-9}$	8.86336	1.54279
1pc	5.69×10^{51}	9.55×10^{12}	$mc^2+8.56\times10^{39}$	$1+4.8\times10^{-8}$	8.86079	0.154
0.1pc	1.81×10^{51}	3.02×10^{12}	$mc^2+8.56\times10^{40}$	$1+4.8\times10^{-7}$	8.85073	0.031
0.01pc	5.7×10^{50}	9.55×10^{11}	$mc^2+8.56\times10^{41}$	$1+4.8\times10^{-6}$	8.81912	0.0031
0.001pc	1.8×10^{50}	3.02×10^{11}	$mc^2+8.56\times10^{42}$	$1+4.8\times10^{-5}$	8.72103	0.00031
ISCO launch 6.9×10^{-8}	1.4985 $\times10^{48}$	2.51179 $\times10^{9}$	mc^2+?	1	One marginally stable Orbit=2.135×10^9m	

Table 4: The Inner Unstable CO and Outer Stable CO and the Marginally Innermost Stable CO in Kerr Metric

Inspection of Table 4 tells us that as Angular Momentum of the test particle is reduced the two circular orbits converge. Eventually at $l/c(m)\rightarrow$ spin parameter = a=2.51178×10^9m we obtain coincident roots corresponding to an Energy Minima as shown in Figure 6. This is the Innermost (marginally) Stable Circular Orbit (ISCO) in Kerr Metric.

So we conclude that for pro-grade orbits, ISCO in KERR Metric is 2.13493×10^9m = 0.36×rG.

The Potential Energy Profile for ISCO is shown in Figure 6 covering a spatial range from 1×10^9m to 4×10^9m.

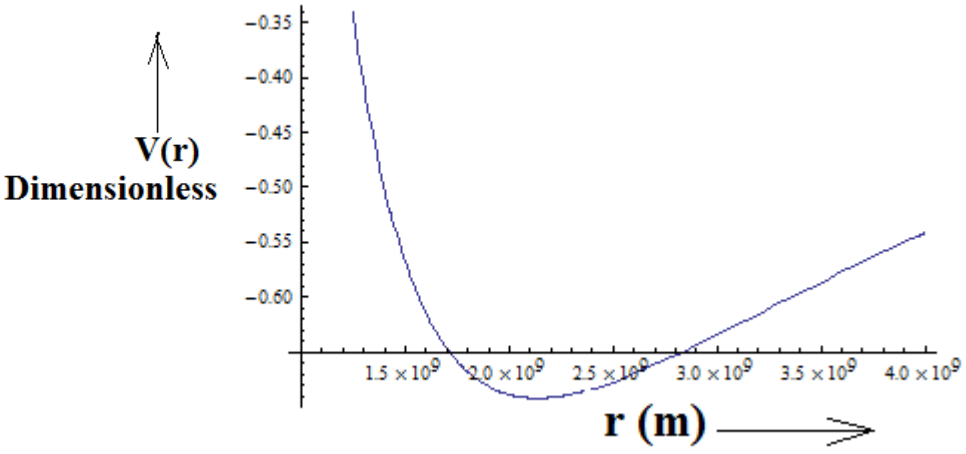

Figure 11: Innermost Marginally Stable Orbit at $0.36r_G$

4.2 Consider the Retrograde Orbit around the Rapidly Spinning Black Hole in NGC 1365

In retrograde orbit, the test particle angular momentum subtracts from the angular momentum of the BH.

I assume l = -K×a. Therefore effective Potential for retrograde massive test particle will be:

$$V_{eff} = (-\kappa\frac{M}{r} + \frac{l^2 - a^2(\varepsilon^2 - 1)}{2r^2} - \frac{M}{r^3}(l - a\varepsilon)^2) /. \{\kappa \to 1, M \to 2.95515 \times 10^9, l \to (-K \times a), a \to 2.51178 \times 10^9, \varepsilon \to 1\} \quad 13$$

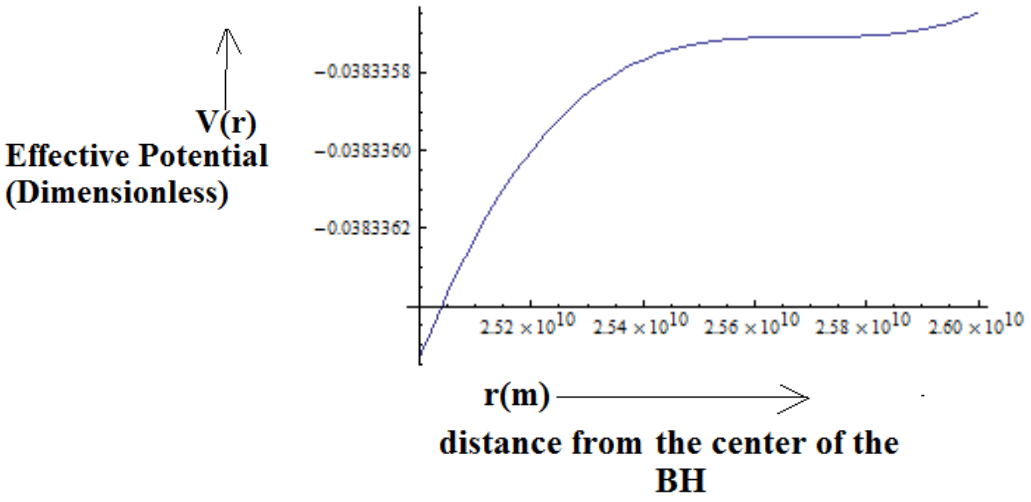

Figure 12: Effective Potential Profile for a Retrograde Massive Particle at Innermost Stable Circular Orbit with l = -4.90625997728496×a. It is more appropriately a Marginally Stable Circular Orbit.

At K = 4.90625997728496, we get a coincident root of the first derivative of (13). The coincident root of the first derivative occurs at :
r=2.56954×10^{10} m=4.34773×r_G

5. Primary-Centric Analysis of Circular Orbits around BH in NGC1365 in Weak-Gravitation Regime

Total Angular Momentum of a binary system is defined as follows:

$$J_T = J_{spin\_A} + J_{Orb} + J_{spin\_b} = C\omega + I_{sec}\Omega + M^*_{sec}a^2\Omega \quad 14$$

Here JT = Total Angular Momentum of the Binary System which is conserved through out the evolutionary history the Binary System. In our case the binary system is a massive particle of solar mass M_Θ = 1.99×10^{30}Kg launched at a given point in NGC 1365 into an orbital path around the BH at the center of NGC1365. Table 5 gives the initial angular momentums of the BH and the massive test particle which is conserved and which decides the circular orbit and which in Primary-centric terminology is the triple synchrony orbits or Clarke's Orbits.

At the circular orbit stage, which is referred to as Clarke's Orbits, the system is in triple synchrony state namely:

$$Black\ Hole\ Spin\ Period = Test\ Particle\ Spin\ Period = Orbital\ Period\ of\ the\ Test\ Particle \quad 15$$

So at Circular Orbit/Clarke's Orbit Stage:

$$\omega_{BH} = \Omega_{test\ particle} = \Omega_{orbital\ period} \quad 16$$

According to Primary-centric Analysis, co-evolving Binary will have a constant total Angular Momentum JT through out its tidally evolving history. Total Angular Momentum is defined as in (14).

In a tidally evolving binary there are two possibilities. The secondary is initially at aG1 which will be shown to be Energy Maxima. This is highly unstable and any disturbance such as solar wind or cosmic radiation can cause it to tumble either short of aG1 or long of aG1.

If the secondary falls short of aG1 then it is trapped by in-spiral path which is a contracting path hence doomed for destruction. Therefore this in-spiral path is referred to as death-spiral. During this in-spiral journey it can either make a head-on collision with the central primary or evaporate as it approaches the central primary by the latter's tidal flexion or it may partially evaporate and partially pulverize by tidal disruption.

If the secondary falls long of aG1 then the secondary is launched on an expanding spiral path by gravitational sling shot effect [25,26]. But during both these possibilities total angular momentum is conserved as long as there is no external torque acting on the system

Because of its constancy, following statement is true:

$$J_T(at\ a = a_{G1}) = J_T(a_{G1} < a < a_{G2}) = J_T(at\ a = a_{G2}) \quad 17$$

Therefore the initial angular momentum satisfies the following condition:

$$J_{T_{initial}} = C\omega + I_{sec}\Omega + M^*_{sec}a^2_{G2}\Omega$$

$$= (C + I_{sec} + M^*_{sec}a^2_{G2})\Omega_{aG2}\ since\ at\ Outer\ Clarke's\ Orbit\ \omega = \Omega = \Omega_{aG2} \quad 18$$

But from Kepler's Third Law:

$$\Omega_{aG2} = \frac{B}{a_{G2}^{3/2}} \quad 19$$

Substituting (17) in JTinitial equation (18) and replacing aG2 by 'A' we get:

$$J_{T_{initial}} = (C + I_{sec} + M^*_{sec}A^2) \times \frac{B}{A^{3/2}} \quad 20$$

By solving for the roots of (20) we get two roots aG1 and aG2. for different values of JTini. These correspond to the Circular Orbits obtained in Schwarzschild Metric and Kerr Metric Effective Potential analysis.

In (20), the most important but uncertain parameter is the polar Moment of Inertia of SMBH namely 'C'. It plays a pivotal role in determining the Circular Orbits but till date we have no accurate formulation for the rotational inertia of SMBH. I have taken the most realistic value of 'C' of SMBH residing in NGC1365.

From http://www.sciencepubnet/report we have the following formulation:

$$P_{spin_{SMBH}} = \frac{A_{SMBH}}{5ac} \quad A$$

where (a)spin parameter in Length Dimension and c is the velocity of light in vacuum.

From Introductory Lectures on Black Hole Thermodynamics, by Ted Jacobson, Institute of Theoretical Physics, University of Uterecht, Section 1.6.1. is devoted to Application of Area Theorem. It gives the area of the event horizon as follows:

$$A_{SMBH} = 8\pi M\left(M + \sqrt{M^2 - \frac{J^2}{M^2}}\right) \quad B$$

Taking the system parameters from Table 3 namely:

$$M \to 2.95515 \times 10^9 m;\ \frac{J}{M} \to 2.48223 \times 10^9 m;\ a \to 2.51178 \times 10^9 m; \quad C$$

Substituting the parameters given in (C) in (B) we get the surface area of the event horizon as:

$$A_{SMBH} = 3.38581 \times 10^{20} m^2; Substituting\ this\ in\ (A) we\ get\ P_{spinSMBH} = 89.927 s;$$

Risalliti et.al. have accurately determined the dimensionless spin parameter which yields the angular momentum of SMBH to be:

$$a = \frac{cJ}{GM^2} = 0.84\ which\ yields\ J(angular\ momentum\ of\ SMBH)$$

$$= 3.52429 \times 10^{54}\frac{Kg-m^2}{s} = C \times \omega \qquad D$$

From (D), polar moment of Inertia of SMBH = C = 4.23702×10^{55}Kg-m^2 ; E

Polar Moment of Inertia of the massive test particle is:

$$I = 0.4M_{\odot}R_{\odot}^2 = 3.85041 \times 10^{47}Kg-m^2 \qquad F$$

Risaliti et.al.(2013) observed the center of NGC1365 through X-Ray Telescope namely XMM-Newton Observatory launched by European Space Agency and through Nuclear Spectroscopic Telescopic Array (NuSTAR) launched by NASA [20].

By measuring the high energy light emitted by iron atoms, telescopes were able to trace the motion of the inner edge of the flat, rotating accretion disk that circles NGC1365's SMBH and funnels gas into the inner region within the event horizon of the SMBH.

Substituting (E), (F), M^*_{sec} = 1.99×10^{30}Kg and $J_{T\ initial}$ = J*(initial angular momentum of SMBH=2.96173×10^{54}Kg-m^2/s)+L*(angular momentum of the massive target particle launched at the edge of the Galaxy = 2.54769×10^{53}Kg-m^2/s) in (20) we get the two Clarke's Orbits:

$$a_{G1} = 3.58525 \times 10^{9}m\ \ and\ \ a_{G2} = 9.83686 \times 10^{21}m$$

Just as the circular orbits in Kerr Metric Effective Potential correspond to inner unstable circular orbit having Energy Maxima and outer stable circular orbit having Energy Minima. In a like-wise manner it is shown in Figure 8 and Figure 9 that inner Clarke's Orbit corresponds to Total Energy Maxima and outer Clarke's Orbit corresponds to Total Energy Minima. Hence inner Clarke is unstable and outer Clarke's Orbit is stable.

Distance of Launch From the center	L*=mr$^{1/2}$B (Kg-m^2/s)	J_T(initial)= L*+J* ($\times10^{54}$Kg-m^2-s^{-1})	Inner Clarke's Orbit($\times10^9$m)	Outer Clarke's Orbit ($\times10^{21}$m)	Inner Unstable CO($\times10^9$m)	Outer Stable CO($\times10^{17}$m)
2000pc	2.54769 $\times10^{53}$	3.2165	3.58525	9.83686	8.86545	617.114
10pc	1.8×10^{52}	2.97973	3.77274	8.44196	8.86398	3.08558
5pc	1.27×10^{52}	2.97443	3.77722	8.41195	8.86336	1.54279
1pc	5.69×10^{51}	2.96742	3.78317	8.37235	8.86079	0.154
0.1pc	1.80×10^{51}	2.96353	3.78648	8.35042	8.85073	0.031
0.01pc	5.7×10^{50}	2.9623	3.78753	8.34349	8.81912	0.0031
0.001pc	1.8×10^{50}	2.96191	3.78786	8.34129	8.72103	0.00031
ISCO launch	7.530127	2.9604	3.78915	8.33279	One marginally stable	
	$\times10^{17}$				Orbit = 2.135×10^9m	

Table 5: Initial Total Angular Momentum for Different Launch Points of the Solar Test Particle and its Circular Orbits and Clarke's Orbits from Kerr Metric and Primary-centric Framework Respectively

From Table 5, it is evident that the two results correspond only in weak gravitation regime when the test particle is very far from the heavy mass concentration in BH.

5.1 Primary-Centric Analysis of Total Energy Profile of the test Solar Particle in NGC1365

From (14), the spin angular velocity is given as follows:

$$\omega(spin\ angular\ velocity) = \frac{J_T}{C} - \frac{(I_{sec} + m^* a^2)}{C}\Omega \quad 21$$

In (21) I have assumed that test particle is in synchronous orbit where secondary spin period is the same as the orbital period of the binary. This will be true only in compact and spectroscopic binaries where tidal effect is strong. Isec = 0.4mRsec2 = the moment of inertia of the secondary around its polar axis. The mass term for the test particle m* is reduced mass that is:

$$m^* = \frac{m}{1 + \frac{m}{M}} = reduced\ mass\ of\ the\ test\ particle. \quad 22$$

From Kepler Third Law as given in (8):

$$\Omega = \frac{B}{a^{3/2}}\ where\ B = \sqrt{G(M+m)} \quad 8$$

Dividing (21) by (8) we get the following:

$$\frac{\omega}{\Omega} = \frac{J_T}{BC} \times a^{3/2} - \frac{I_{sec}}{C} - \frac{m^*}{C} \times a^2 = E \times a^{3/2} - F \times a^2 - \theta_1 \quad 23$$

(23) is Spin/Orbital Angular Velocity equation with constants defined as:

$$E = \frac{J_T}{BC}\ ; F = \frac{m^*}{C} = \theta_2'\ and\ \frac{I_{sec}}{C} = \theta_1$$

Total Kinetic Energy of a Binary is formulated as follows:

$$KE = \frac{1}{2}C\omega^2 + \frac{1}{2}I\Omega^2 + \frac{1}{2}m^* a^2 \Omega^2 = \frac{C\Omega^2}{2}\left[\left(\frac{\omega}{\Omega}\right)^2 + \frac{I}{C} + \frac{M_{sec}^* a^2}{C}\right]; \quad 24$$

Now

$$E = \frac{J_T}{BC} = \frac{(C + I + m^* a_{G2}^2)\Omega_{aG2}}{BC}; \quad 25$$

Since

$$\Omega_{aG2} = \frac{B}{a_{G2}^{3/2}}; \quad 26$$

Substituting (26) in (25) we get:

$$E = \frac{(C + I + m^* a_{G2}^2)}{C} \times \frac{1}{a_{G2}^{3/2}} \quad 27$$

Therefore:

$$E = \left(1 + \frac{I}{C} + \frac{m^* a_{G2}^2}{C}\right)\frac{1}{a_{G2}^{\frac{3}{2}}} \quad 28$$

We define new constants:

$$\frac{I}{C} = \theta_1 (already\ defined\ after\ (23)), \qquad \frac{m^* a_{G2}^2}{C} = \theta_2\ and\ k_1 = (1 + \theta_1 + \theta_2)$$

Substituting these constants in (28) we get:

$$E = (1 + \theta_1 + \theta_2)\frac{1}{a_{G2}^{\frac{3}{2}}} = \frac{k_1}{a_{G2}^{\frac{3}{2}}} \tag{29}$$

Therefore (23) is redefined as follows:

$$\frac{\omega}{\Omega} = \frac{k_1}{a_{G2}^{\frac{3}{2}}} \times a^{3/2} - \left(\frac{m^*}{C} + \frac{I}{C \times a^2}\right) a^2 \tag{30}$$

We change the variable as follows:

$$x = \frac{a}{a_{G2}}$$

Substituting the new variable in (30) we get:

$$\frac{\omega}{\Omega} = k_1 \times x^{3/2} - \theta_2 \times x^2 - \theta_1 \tag{31}$$

Therefore Total Energy is written as follows:

$$T.E. = KE + PE = KE - \frac{GMm}{a} = KE - \frac{GMm}{a_{G2}} \times \frac{1}{x} \tag{32}$$

Substituting (24) in (32) we get:

$$TE = KE + PE = \frac{CB^2}{2a^3}\left[\left(\frac{\omega}{\Omega}\right)^2 + \frac{I}{C} + \frac{m^* a^2}{C}\right] - \frac{GMm}{a_{G2}} \times \frac{1}{x} \tag{33}$$

Carrying out the change of variable in KE expression we get:
Substituting (31) in place of ω/Ω in (33) and substituting θ1 and θ2 in (33) we get:

$$TE = \frac{CB^2}{2a_{G2}^3 x^3}\left[\left(k_1 x^{\frac{3}{2}} - \theta_2 x^2 - \theta_1\right)^2 + \theta_1 + \theta_2 x^2\right] - \frac{GMm}{a_{G2}} \times \frac{1}{x} \tag{34}$$

Plot of TE gives a minima corresponding to Outer Clarke's Orbit= aG2 , a maxima corresponding to Inner Clarke's Orbit and again there is a minima which appears to be the potential well corresponding to the BH in NGC 1365 or it can be treated as a Mathematical Artefact.

Rewriting (31) and substituting the complete expressions of the constants we get:

$$\frac{\omega}{\Omega} = (1 + \frac{I}{C} + \frac{m^* a_{G2}^2}{C}) \times x^{3/2} - \frac{m^* a_{G2}^2}{C} \times x^2 - \frac{I}{C} \tag{35}$$

At x = 1 we should get ω/Ω = 1 and that is what we get exactly from (35).
Also equating J at inner Clarke's Orbit to J at outer Clarke's Orbit we get:

$$(C + I + m^* a_{G2}^2)\Omega_{aG2} = (C + I + m^* a_{G1}^2)\omega_{aG1} \quad 36$$

Simplifying (36) we get:

$$(C + I + m^* a_{G2}^2)\frac{B}{a_{G2}^{3/2}} = (C + I + m^* a_{G1}^2)\frac{B}{a_{G1}^{3/2}} \quad 37$$

Further simplifying (37) we get:

$$\sqrt{a_{G2}}\left(\frac{C + I}{a_{G2}^2} + m^*\right) = \sqrt{a_{G1}}\left(\frac{C + I}{a_{G1}^2} + m^*\right) \quad 38$$

The above algorithm will be used to verify the stability of inner and outer Clarke's Orbits.

In Figure 8 and Figure 9, the Total Energy profile is plotted at inner and outer Clarke's Orbits.

From the Figure 8 and 9, it is clear that Inner Clarke's Orbit at aG1 is an unstable Circular Orbit and Outer Clarke's Orbit at aG2 is a stable Circular Orbit. This is analogous to Kerr's Circular Orbits in weak-gravitation regime.

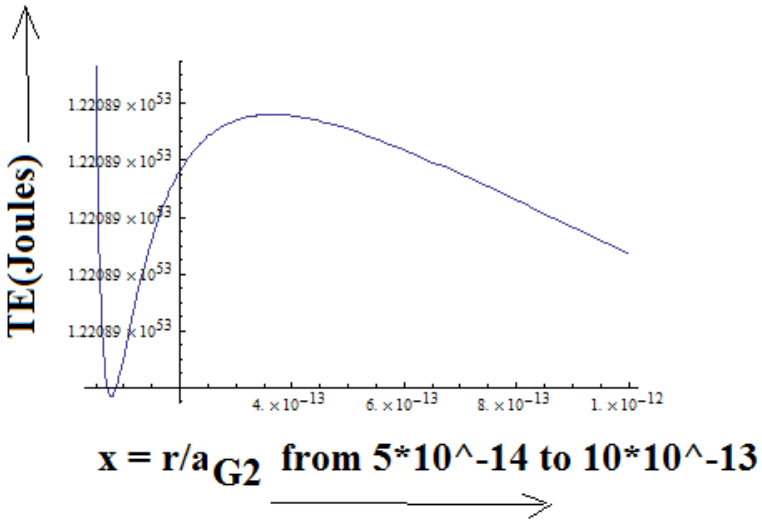

Figure 13: Total Energy Profile of a Star Orbiting SMBH at the Center of NGC1365 at the Inner Clarke's Orbit aG1 and at the Potential Well Created by SMBH at the Center of the Galaxy 1365

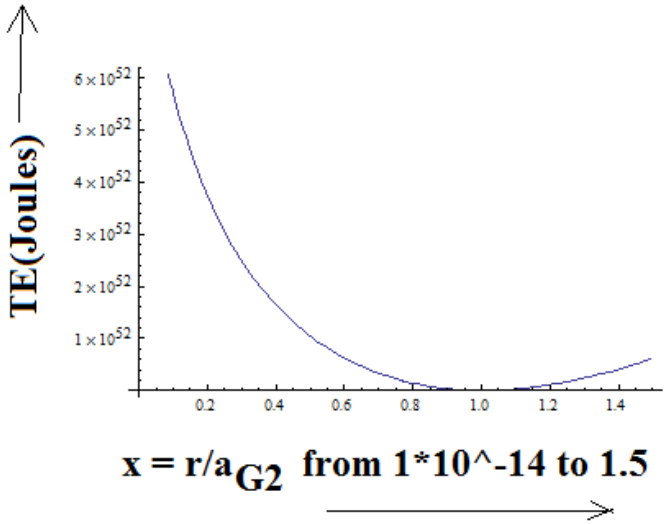

Figure 14: Total Energy Profile of a Star Orbiting SMBH at the Center of NGC1365 at Outer Clarke's Orbit aG2

6. Estimation of SPIN of Black-Hole

The faster a Black Hole spins, ISCO diameter shortens and luminosity of X-ray reflected from the accretion disc increases [27]. Future X-ray, radio and gravitational wave observatories will transform Black Hole spin into a precision tool for astrophysics and it will enable test fundamental theories of gravity.

There are two standard methods of estimating spin of Black Holes [28].

6.1 Method 1

Spectral studies of FeK emission lines emitted from the the inner region of accretion disk around the Black Hole.

6.2 Method 2

Continuum-fitting Method: In this method mass (M), distance D and the angle of inclination ('i') of the accretion disk must be known. There are theoretical and observational evidences that inner disk is truncated abruptly at R (ISCO) [29-31]. Better estimate of spin from R(ISCO) can be made if observed spectrum covers a wide range of energy to include FeK emission ine (~ 6 kev), Compton Hump(~ 10 to 60 kev) and Compton Reflection Component (~ 10 to 20 kev) from the accretion disk. Modelling of reflection component improves the determination of Black Hole spin [32].

Dimension-less spin parameter a* = a/J = (cJ)/(GM^2)
Rin= inner radius of the thin acretion disk (thin disk model) = R(ISCO) is a monotonic function of a* from 6GM/c^2 to 1GM/c^2 wgich corrresponds to a* from 0 to 1. That is inner radius of the disc has reached ISCO.

7. Conclusions

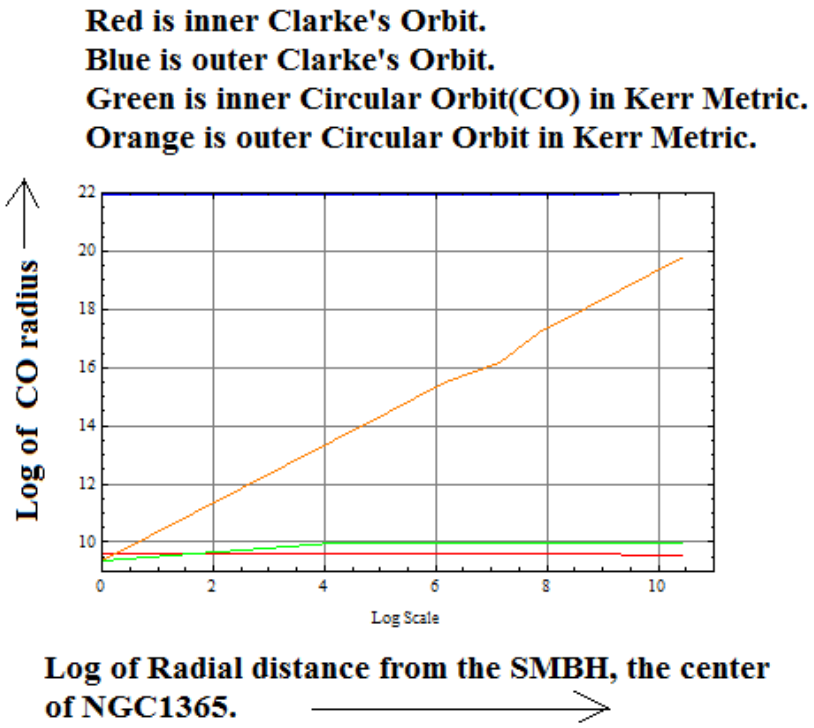

Figure 15: Comparative Graphic Study of the Clarke's Orbits (Blue and Red) Obtained from Primary-Centric Analysis and of Circular Orbits (Orange and Green) Obtained from Kerr Metric

As can be seen in Figure 10, in the far-field from SMBH, the Clarke's Orbits obtained from Primary-centric Analysis are well separated and are of the same range as the COs in Kerr Metric. Therefore the Author says that there is a correspondence in Primary-centric Framework and in Kerr Metric Framework.

On the other hand, as can be seen after a close examination of Figure 10 and 11, in near-field of SMBH, COs obtained from Kerr Metric converge to give rise to a marginally stable CO which is known as Innermost Stable Circular Orbit (ISCO). It is this ISCO which sharply delineates the inner edge of the Accretion Disk. A maximmally spinning SMBH will allow, because of Frame Dragging Effect, a much closer inner edge of the Accretion Disk. In a non-rotating SMBH, ISCO lies at 3Rsch radius whereas in NGC1365, where SMBH is spinning at a spin parameter 'a'=0.84, inner edge of Accretion Disk to lie at 0.36Rsch. It was the precise measurement of this inner edge of the Accretion Disk by Risaliti et.al. using the Event Horizon Radio Telescope which enabled PI to pin down the spin parameter at a = 0.84 [21].

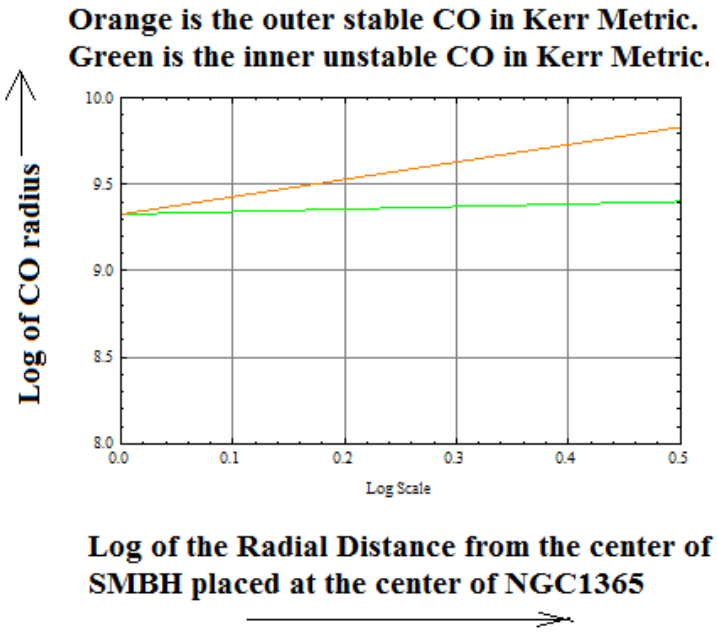

Figure 16: The convergence of Outer Stable CO and Inner Unstable CO in the Immediate Vicinity of SMBH into the Innermost (Marginally) Stable Circular Orbit (ISCO).

This paper has decisively established that Primary-Centric Analysis of Circular Orbits corresponds to the analysis of the same Circular Orbits in Kerr Metric in weak-gravitation regime but in strong gravitation regime Primary-centric Analysis completely fails to arrive at ISCO. Schwarzschild Metric and Kerr Metric account for the space-time curvature in the vicinity of SMBH and Kerr Metric also accounts for Frame-Dragging effect hence it very logically arrives at ISCO which Newtonian framework or a Post-Newtonian Framework like Primary-centric Analysis completely fails to arrive at. Strong or Weak Gravitational Field is defined by the escape velocity of the object under the study.

If the mass of the object is M and radius is R the the escape velocity is defined as:

$$\text{Vescape} = \sqrt{((2GM)/R)} \quad \ldots\ldots\ldots\ldots\ldots\ldots\ldots\ldots\ldots\ldots 39$$

When escape velocity is less than the velocity of light $c = 3\times10^8$ m/sec we have weak gravitational regime and when we have escape velocity equal to or greater than c then we have strong gravitational regime.

Acknowledgement

The Author is indebted to the Director, NIT, Patna, who enabled the holding of a Winter Workshop on General Theory of Relativity from 23rd December 2013 to 3rd January 2014. The Author is also indebted to Virbhadra Swetketu whose brilliant exposition of the subject brought us to an academic level of maturity whereby we are able to work out problems in Strong-Gravitation Regime. The Author is also indebted to University Grants Commission which has been sponsoring his research activities under Emeritus Fellowship Scheme EMERITUS/2012-13-GEN-865/. The Author thanks all the members of the faculty as well as of non-faculty who directly or indirectly helped us in making the Winter Workshop 2013-14 on GR a grand success [32].

Conflict of Interest: There is no conflict of interest, financial or otherwise, with anybody whatsoever.

Data availability: All the data is available within this paper and the references.

References

1. Doeleman, S. S., Fish, V. L., Schenck, D. E., Beaudoin, C., Blundell, R., Bower, G. C., ... & Ziurys, L. M. (2012). Jet-launching structure resolved near the supermassive black hole in M87. *Science, 338*(6105), 355-358.
2. Gezari, S., Chornock, R., Rest, A., Huber, M. E., Forster, K., Berger, E., ... & Price, P. A. (2012). An ultraviolet–optical flare from the tidal disruption of a helium-rich stellar core. *Nature, 485*(7397), 217-220.
3. Sparke, L. S., Gallagher, J. S. (2000). Classification of AGN viewed from different angles. Galaxies in the Universe: An Introduction, published by University of Wisconsin, Madison, and Cambridge University Press.
4. Cantalupo, S., Arrigoni-Battaia, F., Prochaska, J. X., Hennawi, J. F., & Madau, P. (2014). A cosmic web filament revealed in Lyman-α emission around a luminous high-redshift quasar. *Nature, 506*(7486), 63-66.
5. Richstone, D., Ajhar, E. A., Bender, R., Bower, G., Dressler, A., Faber, S. M., ... & Tremaine, S. (1998). Supermassive black holes and the evolution of galaxies. *arXiv preprint astro-ph/9810378.*
6. Libeskind, N. I., Van De Weygaert, R., Cautun, M., Falck, B., Tempel, E., Abel, T., ... & Yepes, G. (2018). Tracing the cosmic web. *Monthly Notices of the Royal Astronomical Society, 473*(1), 1195-1217.
7. Sharma, B. K. (2023). Fractal Architecture of the Universe

Based on Primary-Centric World-View-A Post Co-pernican Conjecture. *J Math Techniques Comput Math, 2*(12), 504-574.
8. Chen, C. T. J., Hickox, R. C., Alberto, S., et. al. (2018). A correlation between Star Formation Rate average Black Hole accretion in the star forming Galaxies. *ApJ, 7731*(1), 3.
9. Hickox, R. C., Myers, A. D., Brodwin, M., Alexander, D. M., Forman, W. R., Jones, C., ... & Mullaney, J. R. (2011). Clustering of obscured and unobscured quasars in the Boötes field: placing rapidly growing black holes in the cosmic web. *The Astrophysical Journal, 731*(2), 117.
10. Koide, S., Shibata, K., Kudoh, T., & Meier, D. L. (2002). Extraction of black hole rotational energy by a magnetic field and the formation of relativistic jets. *Science, 295*(5560), 1688-1691.
11. Van der Klis, M. (1989). Quasi-periodic oscillations and noise in low-mass X-ray binaries. *Annual review of astronomy and astrophysics, 27*(1), 517-553.
12. Tran, H. D. (2003). The unified model and evolution of active galaxies: Implications from a spectropolarimetric study. *The Astrophysical Journal, 583*(2), 632.
13. Hubeny, I., Blaes, O., Krolic, J. H., Agol, E. (2001). Non-LTE models and Theoretical Spectra of Accretion Disks in active Galaxies Nuclei IV: Effects of Compton Scattering and Metal Opacities. *ApJ, 559*, 680-702.
14. Fabian, A. C., Celotti, A., Blundell, K. M., Kassim, N. E., & Perley, R. A. (2002). The properties of the X-ray holes in the intracluster medium of the Perseus cluster. *Monthly Notices of the Royal Astronomical Society, 331*(2), 369-375.
15. Liu, B. F., Qiao, E. (2022). Accretion around BH: The geometry and Spectra. *iScience, 25(*1), 103544.
16. Brenneman, L. W., & Reynolds, C. S. (2006). Constraining black hole spin via X-ray spectroscopy. *The Astrophysical Journal, 652*(2), 1028.
17. Mniutti, G. et.al. (2009). An INTERMEDIATE BH spin in the NLSI Galaxy SWIFT J2127.4+5654 chaotic accretionor spinenergy extraction?. *Monthly Notices of Royal Astronomical Society, 398*, 255-262.
18. Reynolds, C. (2013). Measuring BH spin using X-ray Reflection Spectroscopy. *arXiv 1302.3260 v2 (ASTRO PHY).*
19. Parkar, M. L., Wilkins, D. R., Fabian, A. C., et.al. (2014). The NuStar spectrum of of Markarian 335: Extreme Relativistic effects within two gravitational radii of the Event Horizon. *Monthly Notices of Rpyal Astronomical Society, 443*(2), 1723-1732.
20. Stern, D., Lansbury, G. B., Assef, R. J., Brandt, W. N., Alexander, D. M., Ballantyne, D. R., ... & Zhang, W. W. (2014). NuSTAR and XMM-Newton observations of luminous, heavily obscured, WISE-selected quasars at z∼ 2. *The Astrophysical Journal, 794*(2), 102.
21. Risaliti, G., Harrison, F. A., Madsen, K. K., Walton, D. J., Boggs, S. E., Christensen, F. E., ... & Zhang, W. W. (2013). A rapidly spinning supermassive black hole at the centre of NGC 1365. *Nature, 494*(7438), 449-451.
22. Reis, R. C., Reynolds, M. T., Miller, J. M., & Walton, D. J. (2014). Reflection from the strong gravity regime in az= 0.658 gravitationally lensed-quasar. *arXiv preprint arXiv:1403.4973.*
23. Brenneman, L. (2013). Measuring supermassive black hole spins in active galactic nuclei. *arXiv preprint arXiv:1309.6334.*
24. Done, C., Jin, C., Middleton, M., & Ward, M. (2013). A new way to measure supermassive black hole spin in accretion disc-dominated active galaxies. *Monthly Notices of the Royal Astronomical Society, 434*(3), 1955-1963.
25. Sharma, B. K., Ishwar, B., & Rangesh, N. (2009). Simulation software for the spiral trajectory of our Moon. *Advances in space research, 43*(3), 460-466.
26. Sharma, B. K. (2011). The Architectural Design Rules of Solar Systems Based on the New Perspective. *Earth, Moon, and Planets, 108,* 15-37.
27. Reynolds, C. S. (2019). Observing black holes spin. *Nature Astronomy, 3*(1), 41-47.
28. Kumar, R., Bhattacharyya, S., Bhatt, N., & Misra, R. (2022). Estimation of spin and mass of the black hole in MAXI J1348–630 from the soft state using NICER and NuSTAR observations. *Monthly Notices of the Royal Astronomical Society, 513*(4), 4869-4874.
29. Gierliński, M., & Done, C. (2004). Black hole accretion discs: reality confronts theory. *Monthly Notices of the Royal Astronomical Society, 347*(3), 885-894.
30. Abe, X., Fukazawa, Y., Kubota, D., et. al. (2005). Emission of the Blac Hole Candidate 4U. *PASJ, 57,* 629.
31. McClintock, J. E., Remillard, R. A., Rupen, M. P., Torres, M. A., Steeghs, D., Levine, A. M., & Orosz, J. A. (2009). THE 2003 OUTBURST OF THE X-RAY TRANSIENT H1743− 322: COMPARISONS WITH THE BLACK HOLE MICROQUASAR XTE J1550− 564. *The Astrophysical Journal, 698*(2), 1398.
32. Zhao, X., Gou, L., Dong, Y., Zheng, X., Steiner, J. F., Miller-Jones, J. C., ... & Feng, Y. (2021). Re-estimating the Spin parameter of the black hole in Cygnus X-1. *The Astrophysical Journal, 908*(2), 117.